THE ASTROPHYSICAL JOURNAL, 435:L43–L46, 1994 November 1

WFPC2 OBSERVATIONS OF THE DOUBLE CLUSTER NGC 1850 IN THE LARGE MAGELLANIC CLOUD[1]

R. GILMOZZI,[2,3] E. K. KINNEY,[2] S. P. EWALD,[4] N. PANAGIA,[2,3,5] AND M. ROMANIELLO[6]
Received 1994 June 15; accepted 1994 August 15

ABSTRACT

HST-WFPC2 optical and ultraviolet imaging observations of the young double cluster NGC 1850 in the LMC are presented. The main cluster, NGC 1850A, is a globular-like cluster and has an age of 50 ± 10 Myr, while the subcluster, NGC 1850B, which is more loosely distributed, is very young at 4.3 ± 0.9 Myr. Its young age is confirmed by the detection of a pre–main-sequence population of stars associated to it. The two clusters have considerably different IMF slopes, with the main cluster having a flat slope [$f(m) \propto m^{-1.4 \pm 0.2}$] and the young cluster a much steeper one [$f(m) \propto m^{-2.6 \pm 0.1}$]. The LMC field star population displays a broad range of ages, from $\sim$0.5 Gyr up to more than 4 Gyr.

Subject headings: globular clusters: individual (NGC 1850) — Magellanic Clouds — stars: evolution — stars: luminosity function, mass function — stars: pre–main-sequence

1. INTRODUCTION

NGC 1850 is a young double cluster in the bar of the LMC. It is representative of a cluster population that has no counterpart in the Galaxy: stellar systems having a distribution in age and luminosity similar to those of the galactic open clusters but masses and compactness similar to those of the galactic globular clusters. Its double nature was first noted by Robertson (1974) while detailed studies, based on ground-based observations, have recently been published by Fischer, Welch, & Mateo (1993) and Vallenari et al. (1994).

NGC 1850 was selected for observations with the WFPC2 camera on board the *Hubble Space Telescope* to measure the geometric distortion in the camera. The richness of the cluster ensures an excellent coverage of the full field of view, and yields a correction that provides an astrometric accuracy of 0.1 pixels (0″.01) everywhere within the image (Ewald, Kinney, & Gilmozzi 1994; Gilmozzi et al. 1994). These observations also have provided high-resolution imaging of the cluster in several passbands, from which it has been possible to obtain multi-band photometry of $\sim$9000 stars to produce the most complete and accurate color-magnitude diagrams to date. In addition, the ultraviolet observations have permitted a sharper determination of the properties of the younger subcluster.

2. OBSERVATIONS AND DATA REDUCTION

NGC 1850 was observed with the WFPC2 camera on 1994 March 4 through the F160BW, F170W, F439W, F569W, and F791W filters for 2000, 2000, 1000, 200, and 1000 s, respectively. Each observation was split into two exposures in the ratio 7:3 to identify cosmic-ray events while providing shorter exposures for good photometric measurements of the brightest stars which would be saturated otherwise. In the visual passband (F569W), additional 10 observations at multiple pointings were also obtained to study the geometrical distortion in detail. The observation in the F160BW (Woods) filter is severely vignetted and was used only to assess the amount of contamination from red leak in the F170W filter, an effect that turned out to be negligible for the stars of the cluster.

The observations were processed through the PODPS (Post Observation Data Processing System) pipeline for bias removal and flat fielding. In the cases in which two exposures were taken, the images were combined to minimize the loss of information due to cosmic-ray charge deposition. A threshold of acceptable difference between pairs of images was estimated for all pixels as 20DN. This value is about the shot noise in a nearly saturated pixel, 4095DN. Pixels with readings in excess of this difference were not averaged together to produce the combined image but rather the lower value was adopted after scaling for the exposure time.

Since the field is moderately crowded, preference has been given to aperture photometry following the prescriptions originally put forward by Gilmozzi (1990). In this *Letter* we do not measure the stars in the PC and limit our analysis to the three WF chips. Stellar photometry was done adopting a small aperture radius (2 pixels, i.e., 0″.2) combined with the determination of the sky brightness using the median (in order to minimize contamination by nearby objects) in an annulus with inner and outer radius of 3 and 5 pixels, i.e., 0″.3 and 0″.5, respectively, a choice that in a series of tests proved to be the best combination. Zero-point corrections for the aperture size were determined by doing photometry on isolated stars through various aperture sizes. In the case of the 2 pixel aperture the correction with respect to full aperture is between 0.3 to 0.4 mag, the exact value depending on the filter used. Zero points for the photometry were obtained from WFPC2 calibration observations of the standard star BD +75°325 at the time closest to our observations. They compare very well with the preliminary zero points as reported by the WFPC2 IDT (Holtzmann 1994).

The photometry was performed twice for each frame, i.e., on the uncorrected images as well as on the CR cleaned images. A comparison of the magnitudes in the short and long exposures of each filter shows that the internal accuracy of the photo-

[1] Based on observations with the NASA/ESA *Hubble Space Telescope*, obtained at the Space Telescope Science Institute, which is operated by AURA, Inc., under NASA contract NAS 5-26555.

[2] Space Telescope Science Institute, 3700 San Martin Drive, Baltimore, MD 21218.

[3] Affiliated to the Astrophysics Division of the Space Science Department of ESA.

[4] California Institute of Technology, 170-25, Pasadena, CA 91125.

[5] On leave from University of Catania, Italy.

[6] Dipartimento di Fisica, University of Pisa, Piazza Torricelli 2, I-56100 Pisa, Italy.

metry is of the order of 0.02 mag for bright stars (i.e., 1 mag below the saturation limit) and is still better than 0.1 mag for stars as faint as 5 mag below the saturation level, e.g., for 16.7 and 21.7 mag in the F569W short images, respectively.

The brightest stars in both clusters are moderately saturated (mainly in the F791W filter). We have recovered their photometry by following a method developed by Gilliland (1994). In most cases, this procedure provides photometric measurements accurate to within 0.05 mag.

Since the UV filters distort the stellar images, especially in the CCD corner near the pyramid, the photometry in the ultraviolet has been performed on star lists selected from the UV frame. To minimize the chance of incorrect match for faint stars between UV and optical images, the list of positions was corrected for the scale change between the two wavelengths.

3. RESULTS

Figure 1 (Plate L23) shows a mosaic of all the 100 s F569W observations obtained by combining the five pointings (20″ steppings) used for the determination of the geometric distortion in the WFC (the stepping for the PC case being half that). This composite image, that contains ~12,000 stars, offers a larger view of the cluster's field than the one from which the photometry was derived. Figure 2 (Plate L24) shows a mosaic of the central pointing through the F170W filter. The subcluster is much more prominent in this image, that shows that most of the bright UV stars are located outside of the main cluster and appear to be loosely centered on a small group located some 30″ W of the main cluster.

The color-magnitude (C-M) diagrams, $m(170)$ vs. $m(170)-V$, V versus $(B-V)$, and B versus $(B-I)$, are displayed in Figures 3*a*–3*c*. Note that from now on, we shall refer to the optical bands, as V, B, and I, although their correspondence to the standard Johnson bands is not perfect. The number of stars included in the three CMDs are 2632, 8958, and 8590, respectively. In all cases we can easily see a main sequence extending over a range of more than 10 mag, a well-defined turnoff in the middle of the diagram, and a clear spot of red giant stars located above the MS, in the lower right-hand part of the diagrams.

By fitting the main sequence with models computed by Brocato & Castellani (1993) and Cassisi, Castellani, & Straniero (1994) with $Z = 0.006$ (i.e., ~0.3 times solar), extended to stars more massive than 25 $M_\odot$ with interpolation over Schaller et al. (1992) evolutionary tracks, we estimate an average reddening to NGC 1850 of $E(B-V) = 0.18 \pm 0.02$ and a distance modulus of 18.2. Although the formal error in the distance modulus is only about ± 0.1, the absolute accuracy of the modulus is hard to assess because uncertainties in the zero magnitude scale up to 0.1–0.2 mag. For this reason, the apparent discrepancy with the distance modulus determination by Panagia et al. (1991) for the LMC (18.50 ± 0.13) is not significant at this stage. A detailed discussion of this point will be presented in a future paper (Gilmozzi et al. 1994). To estimate the reddening we adopted a ratio 1:3 of Galactic to LMC extinction in the V band; the derived $E(B-V)$ is not sensitive to the exact fractions adopted for the fit. Instead, we found that there is an intrinsic dispersion of the reddening within the cluster, as clearly shown by the fact that the apparent *horizontal* width of the main sequence in each diagram is highest for $m(170) - V$ and lowest for $(B-V)$. In fact, the measured widths in the almost vertical portions of the CM diagrams (e.g., $B = 16$–19 in Fig. 3*c*) are proportional to the color excess corresponding to each color index, i.e., $\Delta[m(170) - V] \simeq 0.45$, $\Delta[B-V] \simeq 0.07$, and $\Delta[B-I] \simeq 0.17$, while the adopted extinction curve gives $E(1700 - V)/E(B-V) \sim 5$, and $E(B-I)/E(B-V) \sim 2.3$. From this we estimate that the actual extinction may be slightly different from star to star, fluctuating within an interval of $\Delta E(B-V) \sim \pm 0.04$.

Inspecting the CM diagrams we can identify three distinct populations:

1. As shown by the images (see Figs. 1–3) the bulk of the stars constitute a cluster (the *main cluster* or NGC 1850A) which is almost centered in the frames and has a globular-like appearance. Isochrone fitting of this population (see Fig. 3) gives an age of 50 Myr with a possible uncertainty and/or age dispersion of ± 10 Myr. For comparison, Fischer et al. (1993) found an age of 90 ± 30 Myr while Vallenari et al. (1994) estimated 50–70 Myr. The turn-off point, occurring at $M_V \simeq -1.5$ and a color $(B-V)_0 \simeq -0.16$ indicates that the most massive unevolved stars has a mass of 6 $M_\odot$ to within $\pm 7\%$. The maximum mass, as deduced from the giant branch fitting, is 6.6 $M_\odot$. The minimum mass present in this cluster cannot be determined because the cutoff at faint magnitudes, that falls at

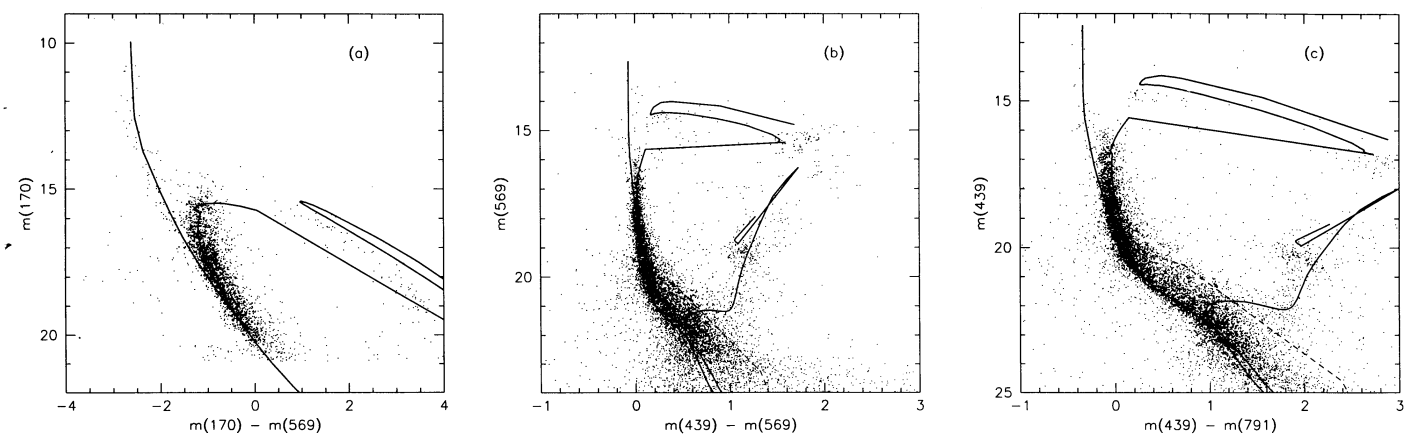

FIG. 3.—Color-magnitude diagrams: (*a*) $m(170)$ vs. $m(170)-m(569)$; (*b*) $m(569)$ vs. $m(439)-m(569)$; (*c*) $m(439)$ vs. $m(439)-m(791)$. Best-fit isochrones for both clusters (4.3 Myr for the young cluster and 50 Myr for the main cluster) as well as an indicative isochrone for field stars (6 Gyr) are shown. The dashed line represents a pre–main-sequence isochrone for an age of 5 Myr and an accretion rate of $10^{-5}\ M_\odot\ \mathrm{yr}^{-1}$ (adapted from Palla & Stahler 1993).

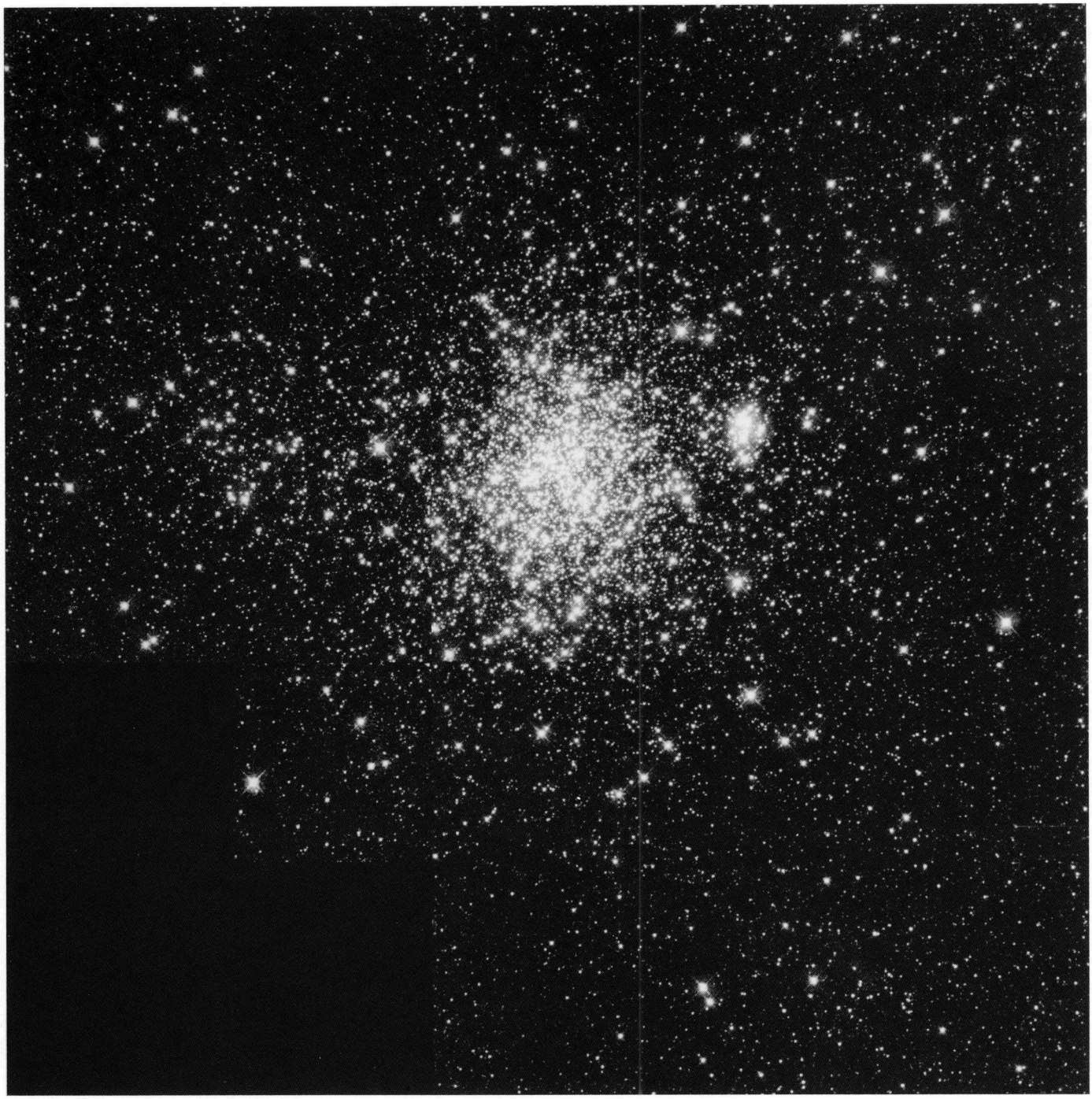

FIG. 1.—Extended mosaic in the F569W band, obtained by combining 200 s observations at five adjacent pointings displaced by 20″. It shows a considerably larger field of view ($\sim 3 \times 3$ arcmin^2) than the one for which photometry was done. North is pointed up at 20° left of the vertical.

GILMOZZI et al. (see 435, L44)

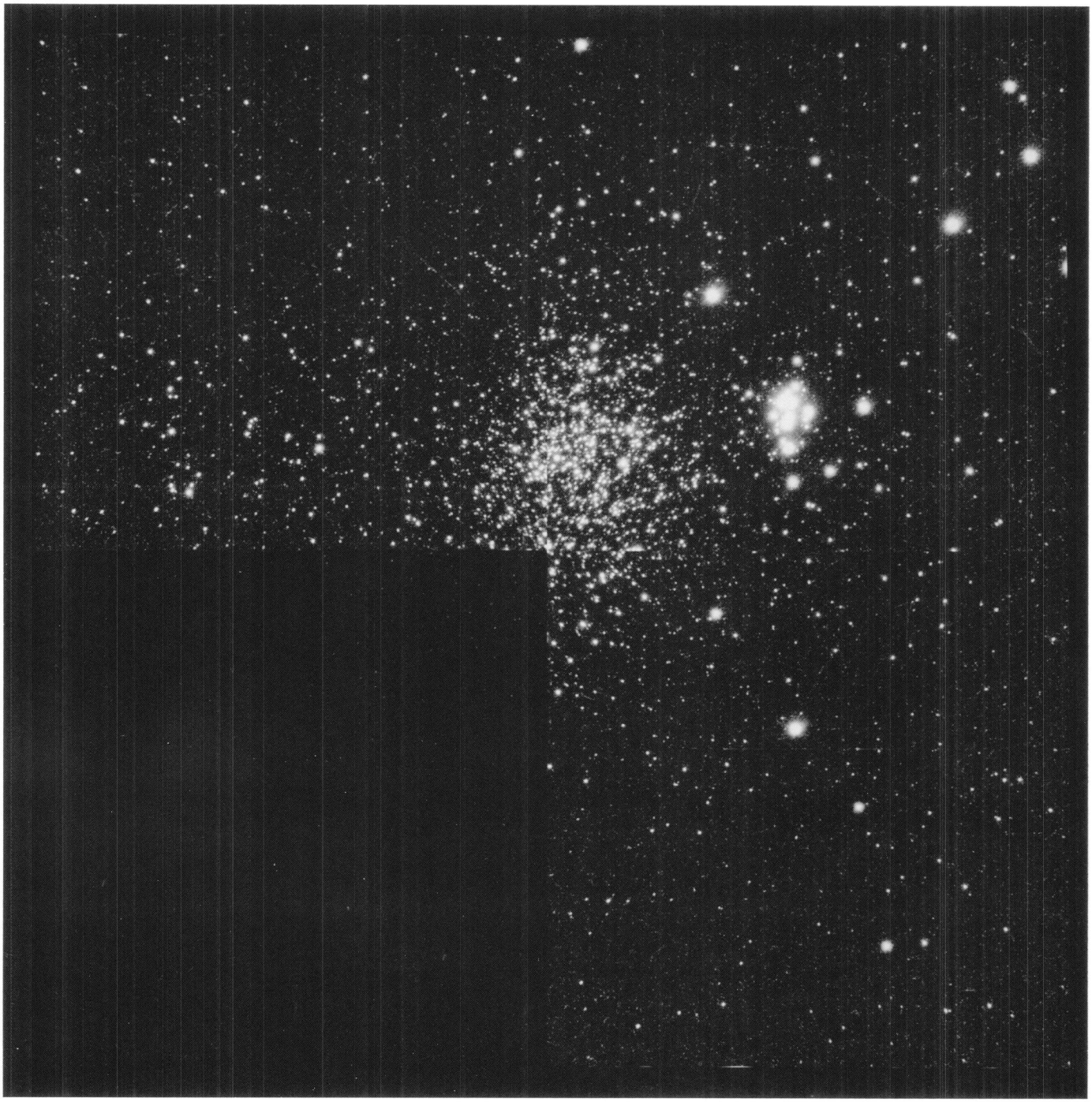

FIG. 2.—Mosaic of the F170W observations. The young subcluster is much more prominent in this figure, which shows that most of the UV bright stars lie outside the main cluster.

GILMOZZI et al. (see 435, L44)

about $M_V \simeq 5$ and corresponds to $\sim 0.9\ M_\odot$, is entirely determined by the detection limits combined with the effects of crowding and confusion.

2. A very young cluster (NGC 1850B or the *young cluster*), whose center is located $\sim 30''$ W of the main cluster. By isochrone fitting of the upper main sequence in the $m(170)$ versus $m(170) - V$ diagram we determined an age of 4.3 ± 0.9 Myr. For the same population Fischer et al. (1993) estimated an age of 6 ± 5 Myr while Vallenari et al. (1994) gave 8–10 Myr. Here, the sharpening in the age determination is predominantly due to the use of UV band photometry that enabled us to define the stellar parameters of the bright and hot stars quite accurately.

About 30 stars of this cluster have an effective temperature above 20,000 K and among them, about half have a luminosity in excess of $3 \times 10^4\ L_\odot$. Using the stellar parameters as compiled by Panagia (1973), we estimate that a total Lyman-continuum photon flux of $\sim 4 \times 10^{49}$ photons s^{-1} is emitted by NGC 1850B, an ionizing flux which may account for the ionization of the H II region N103B (Caplan & Deharveng 1985) in which this cluster appears to be embedded.

The young age of this cluster is confirmed by the presence of a pre–main-sequence population of stars, which are most easily recognized in the B versus $(B-I)$ diagram as an excess over, or to the right of, the main sequence in the range $(B-I) \simeq 0.2$–0.8 and $B \simeq 20.5$–22.5 (see § 4). The excess population can be traced to as high as the 19th magnitude, indicating that stars of masses up to $\sim 3\ M_\odot$ are still in the approaching phase to the MS. For comparison, we show in Figures 3*b*–3*c* an isochrone adapted from Palla & Stahler (1993) model calculations for an accretion rate of $10^{-5}\ M_\odot\ yr^{-1}$ and an age of 5 Myr. The fact that the isochrone appears to envelope quite well the detected PMS population, but corresponds to an older age than the one we derived for the more massive stars, indicates that the average accretion rate is likely to be higher than $10^{-5}\ M_\odot\ yr^{-1}$, possibly by a factor of 2–3.

The fairly uniform spatial distribution of the PMS stars, plus the presence of very bright OB stars as far away as 1′ from the center of the subcluster (cf. Fig. 2), indicate that the young cluster is much looser than the main cluster and has a spatial extent at least comparable to that of the main cluster.

3. A third population is easily identified by the presence of red giants, say, around $(B-I) \sim 2$ and $B \sim 20$. It represents the field stars of the Large Magellanic Cloud. Since field stars are likely to have a considerable spread in ages and in reddening (approximately between the value due to our Galaxy $E_{Gal}(B-V) \sim 0.05$ and at least the maximum value measured for NGC 1850 $E_{max}(B-V) \sim 0.22$) one should expect for them a larger dispersion in the C-M diagrams than for the two clusters. Moreover, the field population should also have a spread of metallicity, thus increasing the spread in the CMDs even further. Indeed the presence of field stars with both a lower reddening and a lower metallicity than that of NGC 1850 is best noticed by the abrupt "fattening" of the lower main sequence starting at about $(B-I) \sim 0.8$ and $B \sim 23$. It is clear that this represents an extension of the lower main sequence toward bluer colors and/or fainter magnitudes, and identifies the turnoff of the bulk of the field stars, suggesting an average age of ~ 4 Gyr. On the other hand, the blue end of the red giant branch, $(B-I) \sim 1.8$ and $B \sim 19.7$, implies the presence of stars as young as 0.5 Gyr, while its red end requires stars with ages in excess of 4–5 Gyr. On this basis we conclude that the field star population has a broad range of ages, say, between 0.5 Gyr and, possibly, as old as 8 Gyr. As an illustration, we display in Figure 3*c* a 6 Gyr isochrone, computed with $Z = 0.001$ (Cassisi et al. 1994), for a reddening $E(B-V) = 0.11$.

4. DISCUSSION

The rich statistics of these measurements deserve a detailed statistical analysis, that is deferred to a future paper (Gilmozzi et al. 1994). Here, we limit ourselves to a simplified analysis to estimate the properties of the initial mass function (IMF) in the two clusters and their relative populations.

The IMF slope for the young cluster may be estimated from the ratio of stars in the upper main sequence and those in the PMS phase. We can identify 64 stars brighter than $m(170) = 17.5$ and, therefore, more massive than $7.2\ M_\odot$. As for the PMS stars, to minimize contamination from field stars we limit the count to B magnitudes brighter than 22.1. Similarly, we limit the count on the bright end at $B = 20.7$ to avoid borderline confusion with the distinction MS-PMS. The interval limits correspond to stellar masses of 1.40–1.99 $M_\odot$.

Also, we have to allow for the presence of field stars which, with ages as young as 0.5 Gyr, may affect the counts severely. The distribution of the field stars near the MS has been deduced from the number of red giants which are present in the region $(B-I) = 1.6$–2.4, $B = 19$–21 (see Fig. 4*a*), assuming that star formation had proceeded at a constant rate in the past 0.5–6 Gyr. Using the models of Brocato & Castellani (1993),

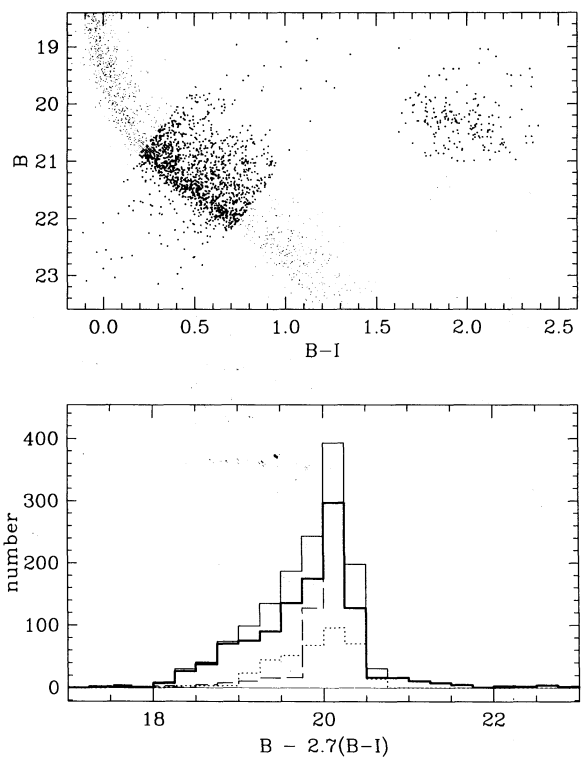

FIG. 4.—*Upper frame:* a blow-up of the B versus $(B-I)$ diagram in which the considered MS-PMS region and the red giant region have been highlighted. Note the well-defined ridge that identifies the MS. *Lower frame:* the distributions of stars along the axis $B - 2.7(B-I)$ which is perpendicular to the MS. The thin line represents the total distribution, the dotted-line histogram is the field star population (see text), the heavy-line histogram is the decontaminated population of NGC 1850A and B, and the dashed-line histogram is the adopted MS distribution for the main cluster. The PMS stars are the excess above the MS, i.e., the difference between the heavy-line and the dashed-line histograms.

the observed number of red giants (192) implies the presence of 387 field stars (on or near the MS) which fall in the region selected for the PMS star count. Figure 4, top panel shows a blow-up of the B versus $(B-I)$ diagram which includes both the red giants and the PMS region. It is apparent that there is a well-defined ridge with a particularly high density of stars, which defined the MS proper, while above the MS the stars extend as far as 1.4 mag, with their number declining gradually. The observed distribution of stars perpendicularly to the MS, i.e., counted as a function of the variable $B - 2.7(B-I)$, is displayed in Figure 4, bottom panel (thin line). The expected distribution of field stars, allowing for a range of reddening of $\Delta E(B-V) = \pm 0.11$, is shown as a dotted-line histogram. Subtracting the field stars from the total distribution we obtain the heavy-line histogram that includes stars belonging to both NGC 1850A and NGC 1850B. The two populations have been separated assuming that the MS stars of NGC 1850A are symmetrically distributed around the peak of the distribution (with $[B - 2.7(B-I)]_{\rm peak} = 20.1$ and a HPFW of 0.75 mag) so that the remaining excess represents the PMS stars of NGC 1850B. In this way we can separate the total 1545 stars into 387 field stars (on and near the MS), 791 MS stars of NGC 1850A, and 367 PMS stars of NG 1850B, with counting uncertainties of about ± 40 for all cases.

Now, from the ratio of upper main-sequence stars to the PMS ones, $N^*(7.2\text{–}40\ M_\odot)/N^*(1.40\text{–}1.99\ M_\odot) = 64/367 = 0.182$ we derive for the IMF of the young cluster an exponent of 2.56 with a formal uncertainty of ± 0.11. This includes only random errors and does not take into account possible systematic effects induced by the model assumptions. With this IMF the total number of NGC 1850B stars brighter than $B = 22.1$ which are present in the B and I frames, are estimated to be $N^*_{\lesssim 22.1}$(young cluster) $\simeq 870$.

The total number of stars brighter than $B = 22.1$, excluding the field red giants, is 4789. Thus, subtracting the near-MS field stars (387), and the YC stars (870), the apparent number of stars of the main cluster is $N^*_{\lesssim 22.1}$(main cluster) = 3532. However, because of crowding, fainter stars near the center of the main cluster are harder to detect and, therefore, the corresponding counts are actually underestimates. The required correction factor can be evaluated by comparing the density of stars in different annuli around the cluster center, up to a distance of 90″, for different magnitude intervals. We find that the distribution is essentially the same, hence unaffected by crowding, for stars brighter than the 19th magnitude but that for fainter magnitudes the apparent distributions become flatter, indicating a loss of detections near the main cluster center. Taking the distribution of the main cluster stars in the magnitude interval 17–19 as a reference (i.e., with a correction factor of unity), we derive correction factors of 1.36 ± 0.11 for the total number of stars brighter than $B = 22.1$, and 1.72 ± 0.14 for stars in the interval $B = 20.7\text{–}22.1$. In this way the ratio of stars in the 1.40–1.99 $M_\odot$ to the total number above 1.40 $M_\odot$ turns out to be $N^*(1.40\text{–}1.99\ M_\odot)/N^*(1.40\text{–}6.6\ M_\odot) = (794 \times 1.72)/(3532 \times 1.36) = 0.284$ which implies an IMF exponent of 1.42 with a formal uncertainty of ± 0.19. This slope falls in the middle of the values proposed for the main cluster (1.3–1.7) by Fischer et al. (1993).

The slopes of the two clusters are quite different from each other and significantly different from the canonical 2.35 Salpeter's IMF slope. It is possible that the large differences in the IMFs between the two clusters originate from the same cause that produced a very compact cluster on one side (the main clusters) and a much looser one (the young cluster) on the other side. If indeed a flatter IMF slope pertains to a tighter cluster (see also Mateo 1993), one should expect the chemical evolution of elliptical galaxies and globular clusters to proceed faster than it does in spiral galaxies and open clusters.

We wish to thank Enzo Brocato for providing access to his code to compute post-MS isochrones, and Francesco Palla for providing pre-MS evolutionary tracks in a digital form. The comments of an anonymous referee were helpful to improve the presentation and the clarity of this paper. M. R. acknowledges the kind hospitality of the STScI during the late phases of this project.

REFERENCES

Brocato, E., & Castellani, V. 1993, ApJ, 410, 99
Caplan, J., & Deharveng, L. 1985, A&AS, 62, 63
Cassisi, S., Castellani, V., & Straniero, O. 1994, A&A, 282, 753
Ewald, S. P., Kinney, E. K., & Gilmozzi, R. 1994, BAAS, in press
Fischer, P., Welch, D. L., & Mateo, M. 1993, AJ, 105, 938
Gilliland, R. 1994, ApJ, 435, L63
Gilmozzi, R. 1990, Core Aperture Photometry with the WFPC, STScI Instrument Report WFPC-90-06
Gilmozzi, R., Ewald, S. P., Kinney, E. K., Panagia, N., & Romaniello, M. 1994, in preparation
Holtzmann, I. 1994, private communication
Mateo, M. 1993, in ASP Conf. Ser., Vol. 48, Proc. Lick/Santa Cruz Summer Workshop on The Globular Cluster-Galaxy Connection, ed. G. Smith & J. P. Brodie (San Francisco: ASP), 387
Palla, F., & Stahler, S. W. 1993, ApJ, 418, 414
Panagia, N. 1973, AJ, 78, 929
Panagia, N., Gilmozzi, R., Adorf, H.-M., Macchetto, F. D., & Kirshner, R. P. 1991, ApJ, 380, L23
Robertson, J. W. 1974, A&AS, 15, 261
Schaller, G., Schaerer, P., Meynet, G., & Maeder, A. 1992, A&AS, 96, 269
Vallenari, A., Aparicio, A., Fagotto, F., Chiosi, C., Ortolani, S., & Meylan, G. 1994, A&A, 284, 447